CALIFORNIA INSTITUTE OF TECHNOLOGY

Lindhurst Laboratory of Experimental Geophysics
Seismological Laboratory 252-21, 1200 E. California Blvd.
Pasadena, CA 91125

Thomas J. Ahrens
Professor of Geophysics

March 4, 2004

"Impact Processes in the Solar System"

NASA NAG5-10198

Final Report

January 1, 2001 to December 31, 2003

Thomas J. Ahrens
Principal Investigator

cy: Dr. Stephen Saunders (NASA)
Adrian Jefferson, NASA Grants Officer
ONR, San Diego
NASA Center for Aerospace Information, Hanover MD
Spons. Res.
Patents Office
Project Accounting (letter only)

E-MAIL: tja@caltech.edu • TELEPHONE# (626) 395-6906 • FAX# (626) 564-0715, 568-0935
WEB ADDRESS: http://www.gps.caltech.edu/~ahrens

1. Impact-induced Research Damage and Shock Attenuation in Solid and Porous Planetary Materials

Our laboratory has previously conducted impact fracture and dynamic failure tests. Polanskey and Ahrens [1990] mapped the fractures from a series of laboratory craters (Fig. 1) and Ahrens and Rubin [1993] inferred that the usually further extending radial cracks resulted from tensional failure during the compression of the shock propagation. The radial spreading induced by the particle velocity field caused the stresses perpendicular to the shock front to become sufficiently large and tensile. This induces "radial fractures." The concentric fractures (Fig. 1) are attributed to the tensional failure occurring after the initial compressive phase. Upon radial propagation of the stress wave the negative tension behind the stress-wave front caused failure along the quasi-spherical concentric fractures. The near-surface and spall fractures are attributed to the fractures described by Melosh [1984]. These are activated by impact and can launch relatively unshocked samples of planetary surfaces to speeds exceeding escape velocity. In the case of Mars, some of these surface samples presumably become the SNC (Mars) meteorites.

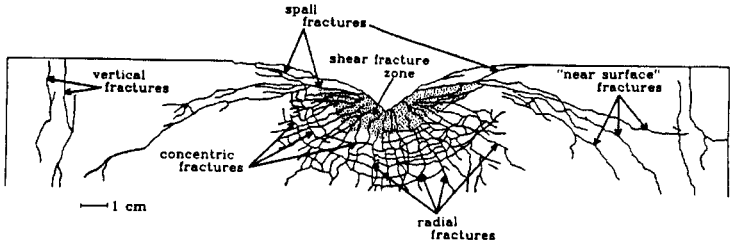

Fig. 1. Cross-section of laboratory impact crater in San Marcos gabbro, demonstrating four types of crack failure (after Polanskey and Ahrens [1990]).

To measure shock tensile or spall strength in planar dimensional geometry, we use the experimental procedure and wave interaction shown in Figs. 2. Later refinement of this method uses ultrasonics to quantify the P- and S- velocity deficits induced by cracks. This allows definition of the onset of fracture and spall fragmentation for different duration tensile stresses. For example, in Fig. 3, we show new data for Coconino sandstone. This rock unit underlies Meteor Crater, Arizona, and according to the refraction survey of Ackerman et al [1975], the unit contains a ~ 1 km diameter by 1 km depth low-velocity zone, presumably due to intense cracking or, failure, in other modes of the sandstone.

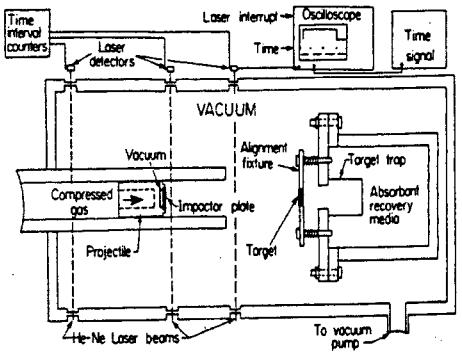

Fig. 2. Sketch of muzzle area of gun showing recovery tank, sample holder, and alignment fixture. The velocity of the projectile is determined both by the travel time between laser beams and by the duration of the interruption of the third beam by the projectile. After impact the sample breaks its support and flies freely into the target trap, where it is protected from further damage [*Cohn and Ahrens*, 1981].

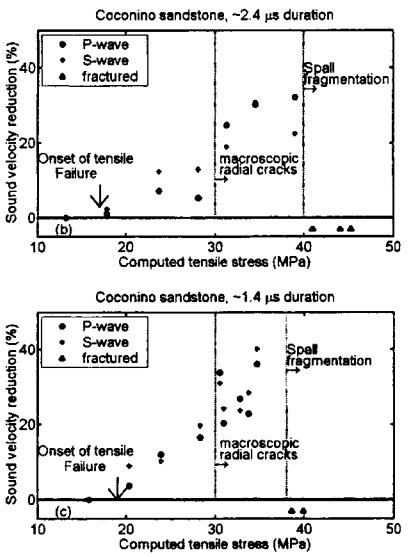

Fig. 3. Velocity measurements of Coconino sandstone for (a) 2.4 μs and (b) 1.4 μs experiments. Dashed lines indicate pressures above which macroscopic radial and spall fragmentation occurred [*Ai and Ahrens*, 2003].

In order to address how tensile failure in one-dimensional planar experiments translate into three-dimensional impact experiments such as those of Fig. 1, we have also developed a tomographic inversion methodology (Fig. 4) for mapping (within a rock target) velocity deficits attributed to cracking using a series of ultrasonic source stations and 24 receiver stations. The tomographic inversion provides low resolution imaging of the severely damaged rock in the region impacted (Fig.5). The less damaged data obtained of Fig. 5 is obtained by dissecting the target into a series of zones measuring the velocity in each subsample. As shown by the figure, these methods compare favorably. Previously, Benz and Asphaug [1995] used the SPH-Weibull strength-flaw model to fit results obtained for Ahrens and Rubin [1993] for a substantially more energetic impact in gabbro (Fig. 7). Initial results indicate that the laboratory and field data may be synthesized to describe damage beneath impact craters on the Earth and planets and with increasing crater size, both in the strength and gravity regime (Fig. 6).

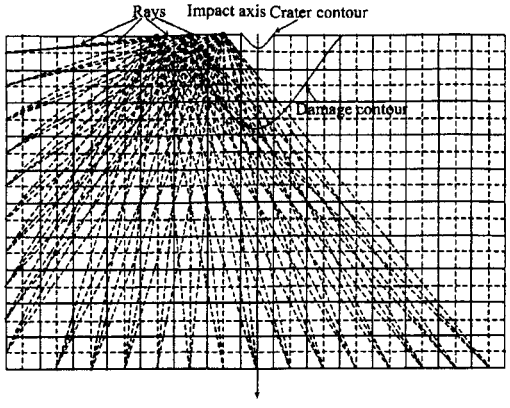

Fig. 4. Tomographic ray diagram. Three stations on upper surface site of pulsed excitation of compressional waves. Wave detection stations (24) along left side and bottom of target block interrogated target along diagonal dashed lines (rays). One-centimeter inversion grid, crater and damage contours are also shown.

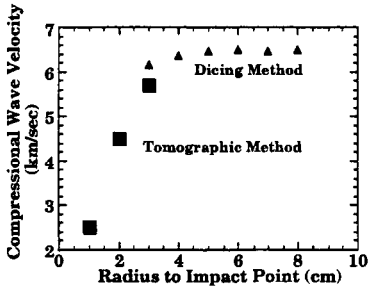

Fig. 5. Compressional wave velocity below strength-controlled impact craters in rock. Tomographic inversion results are seen to delineate heavily damaged region beneath crater whereas dicing method provides complimentary data for deeper, less damaged, rock.

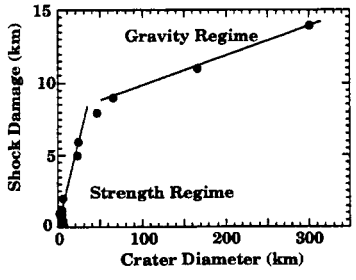

Fig. 6. Depth of shock damage, versus, crater diameter for terrestrial impact craters. Strength regime corresponds to bowl-shaped strength-controlled simple craters. Gravity regime corresponds to complex (central peaks and multi-ringed) craters that have suffered major failure from gravitational stresses.

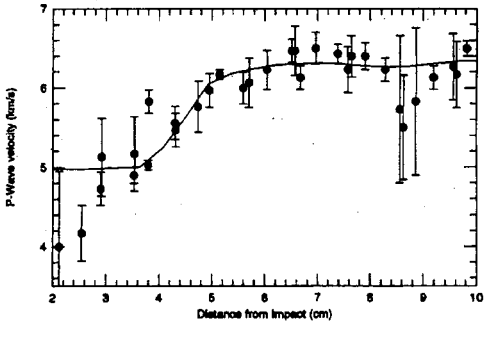

Fig. 7. Compressional wave speed as a function of distance to impact points. Solid dots represent data [*Ahrens and Rubin*, 1993], whereas the results of SPH simulations are indicated by the solid line [*Benz and Asphaug*, 1995].

2. Shock induced Phase Changes

Collaboration with Professors Paul Asimow and Oliver Tschauner, has brought to bear expertise in analyzing shock recovery products with micro-Raman spectroscopy and high-intensity rotating anode x-ray methods, expertise in indexing crystal structures obtained in shock wave recovery experiments and comparisons to results obtained in the laser heated diamond cell. Our initial study [*Luo et al.*, 2004] represents an attempt to reproduce the recently reported post-stishovite phases with the α-PbO_2 and $CaCl_2$ structures, respectively. Although we obtained yet another phase, the α–PbO_2 and $CaCl_2$ phases were discovered and presumably produced by impact shock in the SiO_2 within the Shergotty (SNC) meteorite.

Starting with crystal quartz and coesite, (synthetically prepared in our laboratories, by Asimow) shocked to 55 GPa, and tridymite which was compressed to 30 GPa and laser heated to 1900 ± 100 K in the diamond cell (using H_2O as a pressure medium) a new phase of SiO_2 was recovered from three experiments.

The inversion of x-ray and Raman data indicate its density is between 4.18 and 4.35 g/cm^3 and is within the range of stishovite and some post-stishovite phases, but it does not represent one of the known structural forms occurring along the various transformation paths of post-stishovite phases. This phase appears to be transitional between four- and six-fold coordinated silica phases ~5-fold Si^{+4} coordination with O^{-2}. It is closely related to scrutinite-type α-PbO_2-structure.

3. Impact-Induced Volatilization and Speciation

- Ice.

During the last grant we conducted the first shock wave measurements on 100 K ice [*Stewart and Ahrens*, 2003]. Together with previous 263 K ice data we were able to define five distinct regions along the ice Hugoniot: elastic, ice Ih, ice Ih deformation, and transformation to ices VI, VII and liquid water. The critical pressures required to induce incipient melting (0.6, 4.5 GPa) and complete melting (3.7, >5.5 GPa) upon isentropic release from the shock state (for T_0 = 263, 100 K) were revised using calculated shock temperatures and entropy. On account of the >40% density increase upon transformation from ice Ih to ices VI and VII, the critical shock pressures required for melting are factors of 2 to 5 lower than earlier predicted. Consequently, hypervelocity impact cratering on planetary surfaces and mutual collisions between porous cometesimals will result in abundant shock-induced melting throughout the solar system.

- Calculations involving Ice.

An important application of the ice data is our investigation of the results of hydro-code simulations investigating the outcome of cratering onto ice-rich regoliths. We find that for a typical Mars scenario, regolith contains 20%, 100 K ice and silicate more than half the excavated ground ice is melted by the impact shock, (from a 10 km/s silicate projectile), efficiently fluidizing the ejecta blanket (Fig. 8). Thus, we find that all of the impact ejecta for craters on Mars with diameters up to 30 km contain abundant shock melted water. There are no requirements for a Mars history containing liquid water in the regolith to explain the pedestal crater ejecta morphologies on the planet or the icy satellites (that also demonstrate rampart impact craters). We discovered that for Mars, the impact vapour plume expansion is arrested by the atmosphere for small craters (diameter D <7 km) but disrupts the solid ejecta curtain to form complicated ejecta deposits (containing shock-melted water) when D > 7 km. This explains the correlation between crater size and ejecta morphologies for Mars. The number of craters with fluidized ejecta and estimates of ejecta water content imply a lower limit of redistributed frozen

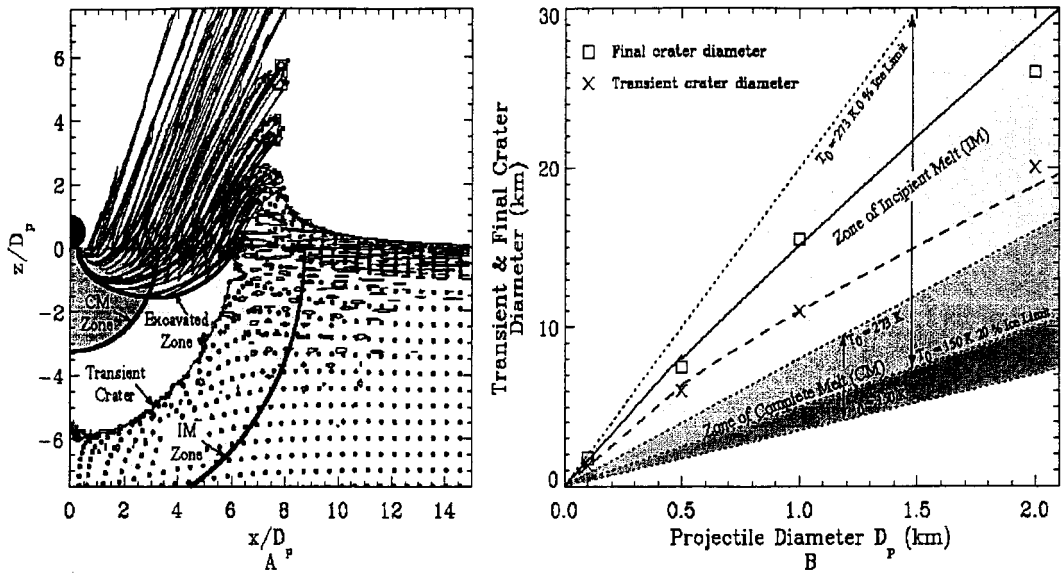

Fig. 8. Regions of crater excavation and shock-induced melting of ground ice. A. Crater excavation zone for 0.5-km diameter projectile impacting at 10 km^{s-1} onto a surface with $\varphi_0 = 0.2$ and $T_0 = 200$ K. Axes scaled by projectile diameter D_p. Trajectory histories shown for Lagrangian tracer particles (□) from within the excavated crater cavity for computation with no atmosphere at 20 sec. B. Transient (x) and final (□) crater diameter as a function of projectile diameter for typical asteroid-derived impactors on Mars. Diameters of hemispherical zones of partial melting of ground ice and complete melting shown for initial temperatures between 150 and 273 K and φ_0 between 0.0 and 0.2. Solid and dashed lines correspond to crater scaling functions in competent rock.

groundwater equivalent to a Mars global layer about 0.5-0.8 m thick. Around 10's km craters on Mars, fluidized ejecta immediately after impact may contain several meters of liquid water, recharging near-surface aquifers. From the crater number density on Mars, the total mass of near-surface (frozen) water is estimated to be equivalent to a 200-m global layer.

- Impact Vaporization of Water from Hydrous Minerals.

We have continued our shock recovery studies of the effect of impact on planetary volatiles. With the late Sam Epstein (with J. Tyburczy), our group published a study [*Tyburczy et al.*, 2001] of the effects of impact on the loss of total H from Murchison meteorite. We obtained large values (43 to 76%) for total H loss from Murchison for initial shock pressures of 10 to 14 GPa. As expected, the theoretical D/H of the shocked residual increased. We found that for the shock residue, δD_{SMOW} $^0/_{00}$ increased from –98.5 (unshocked samples) to values in the ranges –80.0 to –63.0.

In a parallel study with ASU's Michelle Minitti and Laurie Leshin, and others using much smaller samples of terrestrial amphiboles (kaersuterites) (on account of this mineral's carrying most of the sample of Mars' crustal water to Earth in SNC meteorites) and new ion-probe technology, we also obtained an increase of δD_{SMOW} $^0/_{00}$ of 20 to 50 for initial shock compression of ~14 GPa. In the case of the kaesuterite studies, the ion-probe data do not yet give a good measure of the absolute value of D/H nor do they give the expected absolute decreases of H content of the shocked amphibole. More analysis of shocked samples are being conducted.

To provide theoretical guidance for our shock induced vapor speciation experiments, we utilized new thermodynamic and Hugoniot data of metals, minerals and polymers to calculate the entropies associated with thermodynamic states achievable in laboratory impact experiments with projectile velocities up to 6 km/s. [*Shen et al.*, 2003]. Shock and subsequent release processes, being isentropic, make the calculated entropy upon shock compression the most useful measure of the expected final state of the system. However, contrary to Ahrens [1972] and Ahrens and O'Keefe [1972], no optimal entropy-generating distentions[1] for fixed impact velocities were observed.

These results indicate that the studies proposed in which projectile impacts, should yield copious quantities of vapor for minerals of interest such as serpentine, brucite, calcite, dolomite, anhydrite, and gypsum.

We recently reported the first measured shock temperatures in calcite [*Gupta et al.*, 2002]. Of special interest is the 400 to 1350 K temperature deficit observed in this mineral. We propose that this temperature deficit arises from disproportionation of shocked calcite into solid CaO, plus CO_2 (gas) above ~100 GPa along the Hugoniot. These results [*Gupta et al.*, 2003] agree with the conclusion of a reanalysis of our previous shock devolatilization data for $CaCO_3$ [*Yang*, 1996].

We have also further studied [*Gupta et al.*, 2003; *Lyons and Ahrens*, 2002] the shock-induced vaporization of $CaSO_4$ to SO_2, or SO_3, and the production of a global stratospheric aerosol layer which cooled the Earth by 10-15°C for a ~10 year time span at K/T boundary. This resulted in global acifidication of continental land masses, as well as mass extinctions in the upper surface layer of the oceans.

Recently, we have reported the first time-of-flight mass spectra for pyrrhotite, serpentine, olivine, and Murchison meteorite using a 5 ns, N_2 laser pulse to simulate impact on these samples. Some of these data [*Ahrens et al.*, 2003] and recent spectra for $CaSO_4 \cdot 2H_2O$ (gypsum) are shown in Fig. 9. To further provide a theoretical (equilibrium) calculational basis for comparing to ion spectra, we have obtained the assistance of Professor Bruce Fegley (Co-Investigator) in calculating vapor speciation at tropospheric and stratospheric total pressures for the vaporization of $CaSO_4$ (anhydrite) (Fig. 13) and $CaCO_3$.

[1] Distention, m, is the ratio of crystal density, ρ_o, to porous density ρ_{oo}, or $m = \rho_o/\rho_{oo}$.

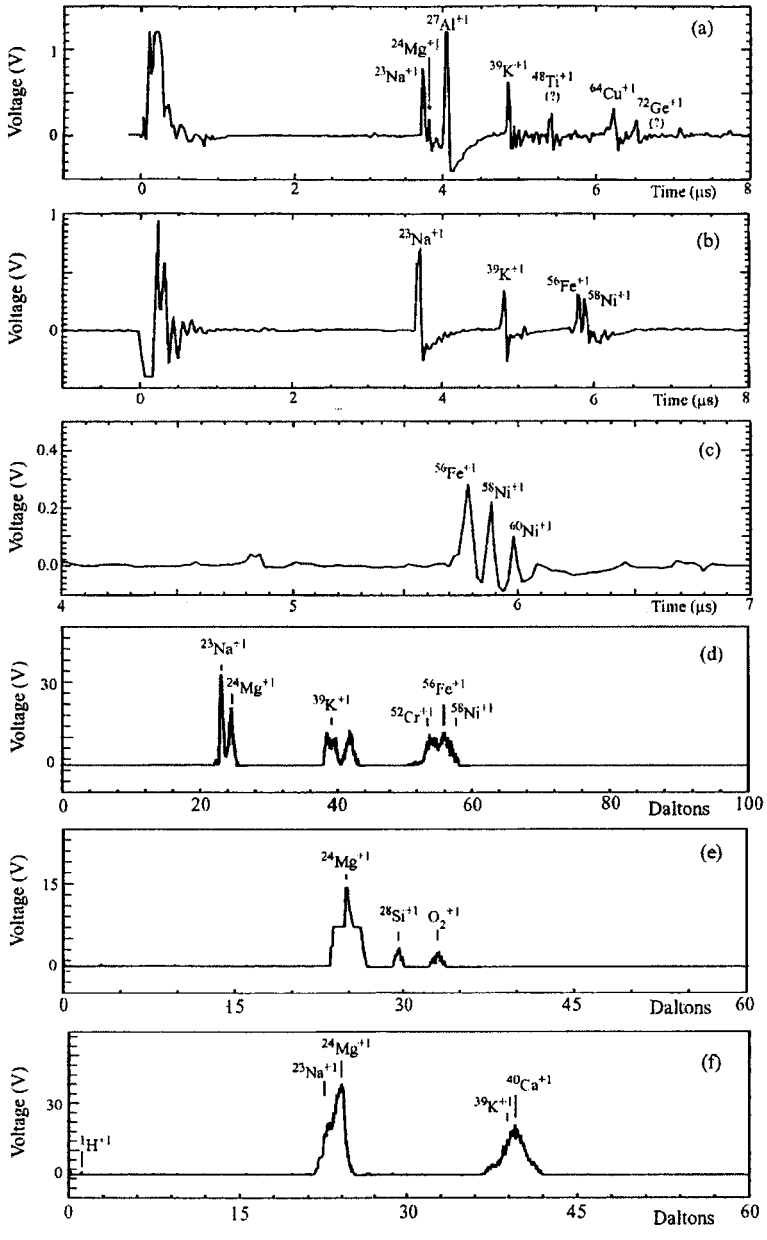

Fig. 9. Single N_2 laser pulse, time-of-flight spectra recorded using multi-channel plate detector (MCP); (a) from Al alloy sample (b) from kamacite (Fe-Ni) at laser power density of 3.45 x 10^9 W/cm^2 (c) from kamacite, at laser power density of 4.5 x 10^9 W/cm^2. (d) from 304 stainless level (8 x 10^7 W/cm^2), (e) olivine (Mg_2SiO_4), 1.8 x 10^7 W/cm2) (f) gypsum ($CaSO_4 \cdot 2H_2O$)(1.6 x 10^7 W/cm^2) [Shen, Ahrens, Gupta, and Beauchamp, unpublished].

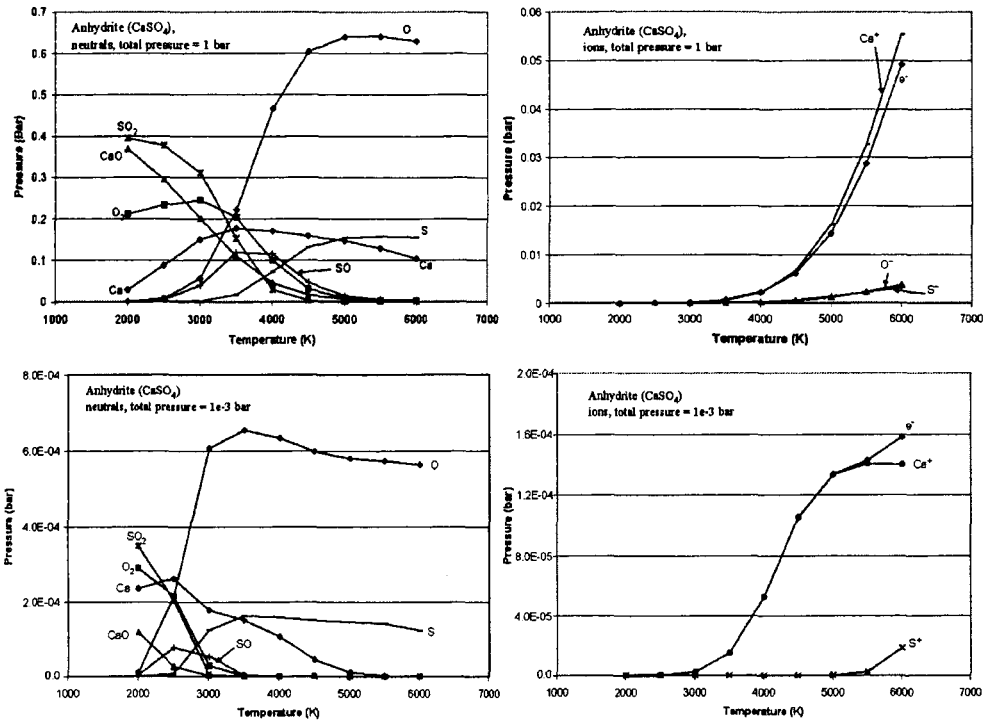

Fig. 10. Calculated equilibrium speciation for anhydrite at normal (a bar) and stratospheric pressure (0.001 bar) versus temperatures using B. Fegley's gas thermodynamics code. Theoretical values are to be compared to TOF manuscript results.

References:

Ackermann, H.D., R.H. Godson, and J.S. Watkins, A seismic refraction technique used for subsurface investigations at Meteor Crater, Arizona, *J. Geophys. Res.*, *80*, 765-775, 1975.

Ahrens, T.J., Shock melting and vaporization of metals, *J. Appl. Phys.*, *43*, 2443-2445, 1972.

Ahrens, T.J., S.C. Gupta, G. Jyoti, and J.L. Beauchamp, Mass spectrometer calibration of Cosmic Dust Analyzer, *J. Geophys. Res. - Planets*, *108, No. E2, 5007, doi:10.1019/2002JE001912*, 1-1 to 1-10, 2003.

Ahrens, T.J., and J.D. O'Keefe, Shock melting and vaporization of lunar rocks and minerals, *The Moon*, *4*, 214-249, 1972.

Ahrens, T.J., and A.M. Rubin, Impact-induced tensional failure in rock, *J. Geophys. Res.*, *98*, 1185-1203, 1993.

Ai, H.-A., and T.J. Ahrens, Dynamic tensile strength of terrestrial rocks and application to impact cratering, *Meteorit. Planet. Sci. - Special Issue (in press)*, 2003.

Benz, W., and E. Asphaug, Simulations of brittle solids using smooth particle hydrodynamics, *Computer Physics Communications*, *87(1-2)*, 253-265, 1995.

Cohn, S.N., and T.J. Ahrens, Dynamic tensile strength of lunar rock types, *J. Geophys. Res.*, *86*, 1794-1802, 1981.

Gupta, S.C., S.G. Love, and T.J. Ahrens, Shock temperature in calcite ($CaCO_3$) at 95 to 160 GPa, *Earth Planet. Sci. Lett.*, *201*, 1-12, 2002.

Luo, S.-N., O. Tschauner, P.D. Asimow, and T.J. Ahrens, A new dense silica phase: a possible link between tetrahedrally and octahedrally coordinated silica, *Amer. Mineral. (in press)*, 2004.

Melosh, H.J., Impact ejection, spallation, and the origin of meteorites, *Icarus*, *59*, 234-260, 1984.

Polanskey, C., and T.J. Ahrens, Impact spallation experiments: Fracture patterns and spall velocities, *Icarus*, *87*, 140-155, 1990.

Shen, A.H., T.J. Ahrens, and J.D. O'Keefe, Shock wave induced vaporization of solids, *J. Appl. Phys.*, *93*, 5167-5174, 2003.

Stewart, S.T., and T.J. Ahrens, Shock Hugoniot of H_2O ice, *Geophys. Res. Lett.*, *30, doi:10.1029/2002GL016789*, 1332, 2003.

Tyburczy, J.A., X. Xu, T.J. Ahrens, and S. Epstein, Shock-induced devolatilization and isotopic fractionation of H and C from Murchison Meteorite: some implications for planetary accretion, *Earth Planet. Sci. Lett.*, *192*, 23-30, 2001.

Yang, W., Impact volatilization of calcite and anhydrite and the effects on global climate from the K/T impact crater at Chicxulub, Ph. D. thesis, California Institute of Technology, Pasadena, CA, 1996.